Real-time microseismic overburden surveillance at the Grane PRM field offshore Norway

S. Bussat[1], M. Houbiers[1] and Z. Zarifi[1] demonstrate how processing and analysis of large amounts of passive data allows for real-time injection monitoring at Grane.

Introduction

Real-time microseismic detection at offshore hydrocarbon fields is on its way to becoming a standard monitoring tool. Recently, increased focus on injection and overburden surveillance for an improved health, safety and environment (HSE) and cost saving has led to this development. Several hydrocarbon fields are already equipped with permanent reservoir monitoring (PRM) systems with seismic sensors permanently installed at the seafloor (Caldwell et al., 2015), and similar installations are planned or under consideration for some other offshore fields. PRM systems are in principle designed for acquiring active time-lapse seismic data 1-2 times per years, and as such, they are not used during most of their lifetime. But apart from active seismic, PRM systems can also be used for recording passive seismic data. With appropriate processing and analysis methods, such as microseismic event detection, the continuous stream of passive data can be converted into useful real-time subsurface information. This results in improved HSE, and therefore a more valuable PRM system.

In 2014, a mini-PRM system with 172 multi-component sensors was installed at the Oseberg field, offshore Norway. The mini-PRM system indeed demonstrated the feasibility of injection and overburden surveillance using real-time passive seismic (Bussat et al., 2016). Despite high installation costs, a cost/benefit evaluation shows net benefits for the Oseberg system owing to better control on waste injection rates.

The next step, and topic of the current paper, is to scale up and transfer the learnings from the small Oseberg system to the large Grane PRM system, so as to enable processing and analysis of large amounts of passive data and allow for real-time injection monitoring at Grane. Compared to the Oseberg case, the microseismic data processing is distributed and optimized to be able to use many more sensors and monitor larger subsurface volumes with increased resolution. Moreover, the detection method is improved from an originally strict semblance-based method to also include signal-to-noise (S/N) analysis of the semblance-weighted stack. Crucial noise filtering is integrated into the real-time processing flow, enhancing the sensitivity of the system and ensuring the best possible detection/localization at any time. Key personnel receive an alert immediately after an event detection. This makes the monitoring fully integrated into the follow-up of the daily operation.

Creating confidence in the monitoring tool is important and therefore its functionality must be verified. In the absence of microseismic events, it is difficult to show that the system really works. Nevertheless, its functionality could be demonstrated by analysing passive seismic data acquired during two well operations. Events detected at reservoir level at one well are used to illustrate challenges in locating the microseismic events in space and to investigate the aperture required for event localization. Microseismic events detected during a plug and abandonment (P&A) operation of another well are used to highlight the importance of noise removal and improved detection methods. Although the P&A-related events are very weak, they have been used to calculate static corrections to further improve the detectability of events.

Beyond operation-related microseismic event detections, the Grane PRM system is used for earthquake detection in an area, remote from conventional seismological stations. Global earthquakes can be detected as well as small local events; even small local events below the detection threshold of the Norwegian National Seismic Network (NNSN) have been detected. A co-operation with NNSN is initiated to provide Grane/Oseberg data for future earthquake detections.

Grane PRM

The Grane field is located offshore Norway, ~200 km west of Stavanger, and has been producing heavy oil since 2003 from a depth of around 1700 m TVDSS. The Grane PRM system was installed in 2013 and is Statoil's second-largest of its kind (Thompsen et al, 2015) covering an area of about 14x4 km^2 with 3458 4-component (4C) sensors trenched into the seafloor (Figure 1). Receiver spacing along the cables is 50 m and cable spacing is 300 m. Active seismic data is acquired twice per year; currently 7 PRM vintages have been acquired. Apart from during the periods of active surveys, passive seismic data are recorded continuously, almost 2.4TB of data every day. The aim is to use these data for monitoring the overburden continuously in real time.

The current production/injection strategy at Grane maintains approximately the initial reservoir pressure and we do not anticipate detection of microseismic events from the reservoir. Nevertheless, a surveillance system for two injector wells is needed. Well G23 is a disposal well for cuttings re-injection (CRI) and it injects into the shallowest sand in the Hordaland formation

[1] Statoil
* Corresponding author, E-mail: sbus@statoil.com

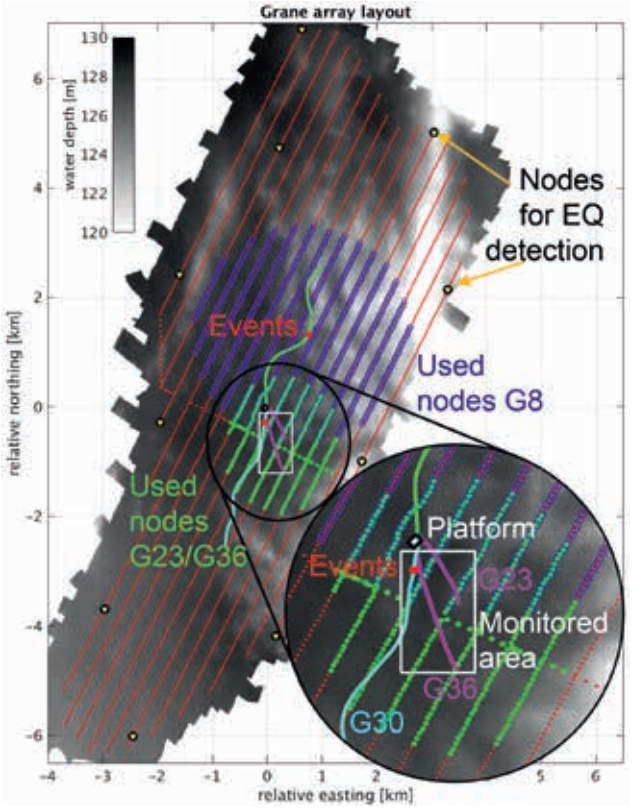

Figure 1 Grane PRM field layout (red lines) showing the used nodes (green) for microseismic real-time surveillance of the injector wells G23 and G30 (magenta lines). The well path of G30 is also indicated (cyan line). Blue nodes indicate nodes used for the study of events from the G8 well (green line). Yellow stars indicate stations currently used for EQ detection. Bathymetry map in the background. Red dots indicate the location of events discussed in this paper.

at 1050 m TVDSS. The second well, G36, is a produced water injector (PWI). It injects into the sand of the Utsira formation at around 900 m TVDSS using a 500m-long horizontal perforation. Monitoring of injection wells is important because onshore disposal of waste is considerably more expensive than offshore. If cuttings cannot be transported to land owing to bad weather, it would result in a drilling stop, with consequently high financial disadvantages. This applies similarly to the produced-water injector, as a loss of the PWI well could result in a production reduction. The two injector wells are located relatively close to each other, and they are simultaneously monitored with a subset of 349 PRM sensors (Figure 1).

With the PRM system and the microseismic detection/localization system in place, injection monitoring is achieved at limited extra costs (mainly for data storage, compute power, and personal costs for follow-up), but with a huge HSE advantage. In addition, we expect an extended lifetime of the injector wells, as the injection can be steered more carefully, based on the occurrence of microseismic events. Therefore, the microseismic surveillance has a very favourable cost/benefit scenario.

In addition to monitoring the G23 and G36 injector wells, we are paying close attention to unexpected situations and events, as the real-time microseismic monitoring is relatively new and we are interested in gaining more experience. One example is the detection of events during a plug and abandonment (P&A) operation in well G30, which by chance is located within the monitored subsurface volume and which will be discussed later.

Verification of the functionality of the system

First experiences from the Oseberg injector indicated that microseismic events occur only during the start-up phase of the injection and the first several injection batches. The amount of microseismic events declines towards zero when injection has been continuing for some time. The start-up phase of the Grane injector wells has not been monitored. Hence, we don't anticipate occurrence of microseismic events for these matured wells, unless the rock formation where fluids are injected becomes too tight (owing to injected particles), the pressure becomes too high, or in the case of caprock failure. The absence of injection-related microseismic events makes it challenging to verify the functionality of the detection system and raises the question of whether the system really works. Therefore, various QC-procedures have been applied to avoid overlooking microseismic events and to increase confidence in the system:

- Synthetic events with different magnitudes are used to define the best processing parameters. The weakest synthetic events had signal-to-noise-ratios (S/N) far below 1 on single traces. Around 30 processing flows (different combinations of stack, semblance, Hilbert transform, automatic gain control (AGC) and S/N ratio) have been tested with multiple input parameters (S/N parameters, down-sampling and different segmentation of data) resulting in a 'global'-search for the best possible processing.
- Testing of various noise removal methods with different parameters prior to microseismic event detection. These methods are tested on data having different noise sources and patterns.
- The detection/localization algorithms are independently implemented in Matlab (for prototyping and testing) and Java (for real-time monitoring), by different software developers. Both implementations are tested against each other, both for real and synthetic events.
- Noise/events from well operations are used for system qualification as shown below. This has resulted in general interest on monitoring drilling operations along drill paths. Despite a very good velocity model for imaging the reservoir, the shallow overburden requires some additional static corrections to improve the detectability. The G30 P&A events are used as an example of how a static correction can been calculated.

Microseismic processing

Every day, a continuous stream of almost 2.4 TB of passive data are recorded with the 3458 multi-component sensors at Grane, at a 2 ms sampling rate. These data are processed with Statoil's inhouse software for microseismic event detection to ensure that the passive data are analysed properly and all necessary information is extracted before permanently deleting them. Statoil's internal software uses distributed processing and would be able to process the entire Grane field if desired, but currently we only use the 349 receivers above the two injectors. The selected receivers are distributed on the seafloor within a radius of 1200 m. Pre-processing of the data consists of rotation of the geophone data, and

applying a frequency filter, an FX median filter (Elboth et al., 2010; Blunda and Chambers, 2013), and a subspace filter (Jones and Levi, 1987), followed by an AGC.

Based on the well-known velocity model, P and S-wave travel times from all receivers to each subsurface point (voxel) in the volume of interest are calculated. For each voxel, the data are then corrected for these travel times (P-wave travel times for the vertical geophone component and S-wave travel times for the horizontal components) and semblance and single-to-noise ratio (S/N) of the semblance weighted stack are calculated. The use of the S/N allows us to detect very small events during periods with less background noise and avoids too many false events during periods with a strong ambient noise. The detection is triggered when two thresholds are exceeded simultaneously, one for the semblance and one for the S/N of the semblance-weighted stack. The values of the two thresholds are chosen such that too many false detections are avoided. A web interface displays relevant well data together with the detected microseismic events and allows even for inexperienced users to quickly QC microseismic detections (Houbiers et al., 2018).

In the marine environment noise removal is crucial. Onshore noise sources are normally very localized and can often be removed by simply rejecting the noise-contaminated sensors. Owing to the sound-conducting water layer, that does not work offshore where all sensors are affected simultaneously by the same noise. The strongest offshore noise source is seismic interference (SI), that is, active seismic shooting within a radius of ~100 km, often occurring during the entire summer half-year, followed by noise from installations (local or neighbouring platforms) or vessels passing by. SI are strong transient signals whereas platform/vessels emit more continuous wave fronts. By applying one or more passes of the subspace filter per cable, both noise sources can be suppressed (Houbiers et al., 2018). The subspace filter applies a time shift to the traces to flatten the strongest incoming noise, removes the largest eigenvalues and reverses the applied time shifts. Figure 2 shows an example where the first pass of the subspace filter suppresses the transient SI noise and a second pass suppresses the continuous platform noise, resulting in an increased S/N of the microseismic event (red arrow).

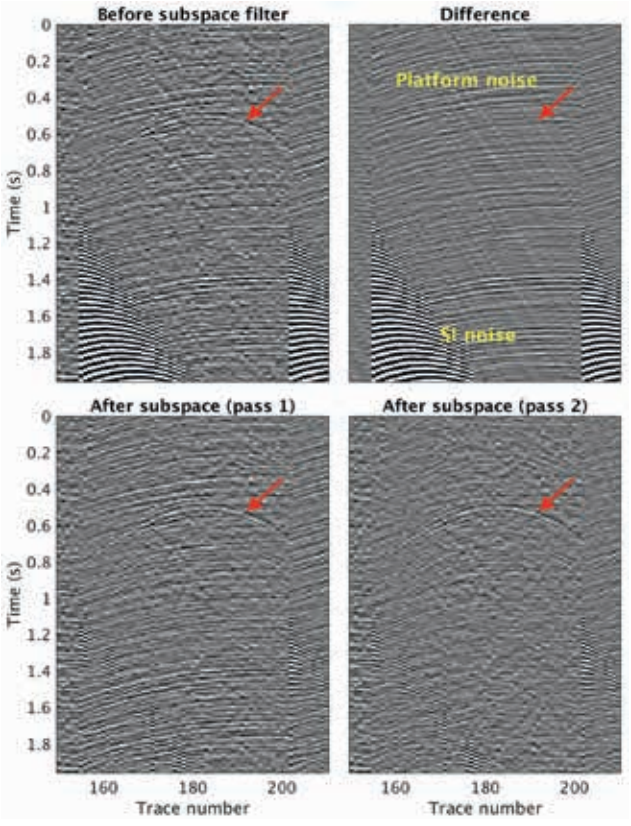

Figure 2 Subspace filter application to raw data (top left), contaminated with SI (suppressed by first pass (bottom left)) and platform noise (suppressed by second pass (bottom right)). The difference image (top right) shows that the microseismic event (red arrow) is not touched by the filter. A 2-45 Hz bandpass and FX median filter have been applied to the raw data.

Example 1: Microseismic at reservoir depth — liner failure at well G8

Two examples from Grane are presented here to demonstrate the benefits and challenges in current microseismic work. The first example represents microseismic events detected during a drilling operation of the G8 well (green well path in Figure 1) in Summer 2015. After the 11 ¾-inch liner (casing string) was set in the reservoir, the drilling team experienced problems entering the liner with the 10.8-inch drill-out bottom-hole-assembly (BHA). An obstruction prevented the BHA to enter further into the 11¾-inch liner. Several unsuccessful attempts were made to clean the liner before a multi-finger caliper finally revealed that the 11¾-inch liner was damaged and possibly parted (Figure 3). The wellbore had to be abandoned and a side track needed to be drilled. The most likely reasons for this liner incident are possible production failure of the liner or a fault movement. At that time, there was no real-time monitoring in place, but the passive seismic data acquired during the incident have been stored and been investigated afterwards. It turned out that prior to the time at which drilling problems were experienced, several microseismic events were detected nearby the location of the damaged liner. If real-time detection of microseismic events would have been in place back then, it would have influenced the decisions of the drilling team, i.e., they could immediately have checked the liner instead of trying to clean it for some days, and money could have been saved.

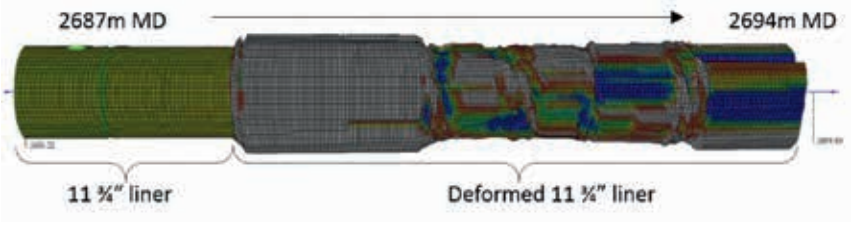

Figure 3 Multi-finger caliper of deformed 11¾-inch liner in well G8.

For microseismic event detection, all 832 sensors within a radius of 2 km from the event location were used (Figure 1). The clearest detected G8 microseismic event is shown in Figure 4. Events consist of both P and S waves with magnitudes up to roughly 0.8 M_W. A high-velocity Shetland layer just below the reservoir creates some depth uncertainties in the imaging. As seen in the 3D S/N volume, there are maxima below the actual event location which create a larger depth uncertainty, while having still a sufficient x-y localization.

Using the P-wave of the strongest G8 event, the depth uncertainty of the event is investigated in more detail. One of the main questions is always: which aperture (offset) is necessary to accurately locate an event? The large Grane PRM array allows us to investigate this in more detail using a real microseismic event example. The microseismic detection is run for only the x-y location of the strongest G8 event resulting in a semblance versus depth curve for each iteratively increased array aperture. We start only using nodes directly above the event and continue until the array contains nodes with maximum offsets of up to 3000 m. Hence, we increase the number of used nodes continuously (Figure 5, left) or we limit the number of nodes to 200 nodes, which are equally distributed over all offsets (Figure 5, right). The cyan curve in Figure 5 shows the depth at which the semblance has its maximum. This curve shows thus how the estimated event depth varies when more and more offsets are included in the semblance computation. For short maximum offsets (below 500 m), estimated depths vary wildly. This is because the short offset traces do not contain the hyperbolic move-out information needed to determine the depth of the event, and as a result, the semblance has a broad peak at small offsets. When including longer offsets, up to the order of the event depth around 1800m, the peak in the semblance becomes more focused, resulting in more reliable and stable depth estimates. Using offsets beyond the event depth seems to provide only small improvements in the depth estimate. The same conclusions also hold when limiting the number of traces to 200, although the semblance panel becomes noisier. This demonstrates that, despite the reduction in stacking power, even a 'mini'-PRM system can provide sufficient depth estimates when the correct aperture size is chosen.

Example 2: Overburden microseismic events from P&A operation of well G30

While listening for microseismic events from the CRI well G23 and the PWI well G36, 306 events have been detected near the G30 well path during a period of seven hours. At that time, a plug and abandonment (P&A) operation was taking place for G30 to prepare it for a new side track. During the P&A process, it must be confirmed that the quality of the cement plug satisfies the requirements. This is done by drilling into it. No microseismic events are expected from such an operation. The unexpected events were detected in real-time because they fall coincidently within the subsurface volume which is used for the injection monitoring (white rectangle in Figure 1).

Figure 6 shows the event with the highest S/N for the semblance-weighted stack. The event is clearly focused in the 3D S/N volume, near the G30 well path, but not visible on the seismic data. It has a semblance of only 8.6%. Although these kinds of events do not occur normally in the real-time monitoring, it was initially questionable whether this event is real, and this in turn raises the general question of when we can trust that detected

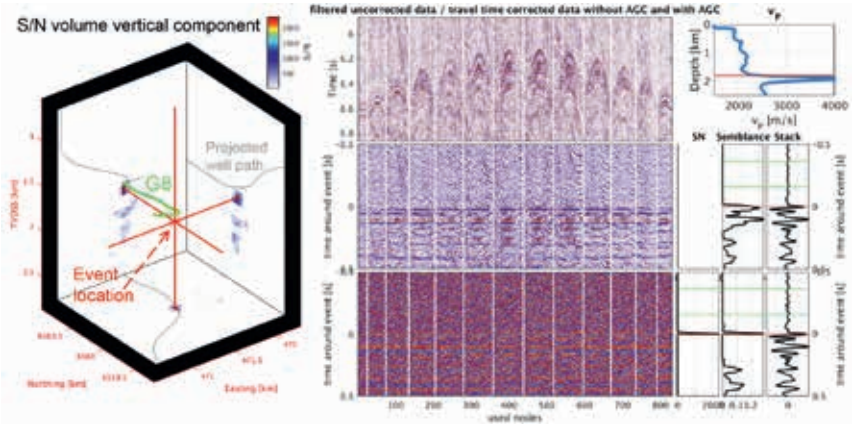

Figure 4 Clearest G8 microseismic event. Shown are slices through the event location within the 3D S/N volume (left), the vertical component (5-40 Hz, top middle) and the travel-time corrected data (without (middle) and with (bottom) AGC). The S/N of the semblance-weighted stack, the semblance and the stacked seismic are shown at the bottom right. The 1D velocity model (top right) shows the high velocity layer below the location of microseismic events (red line).

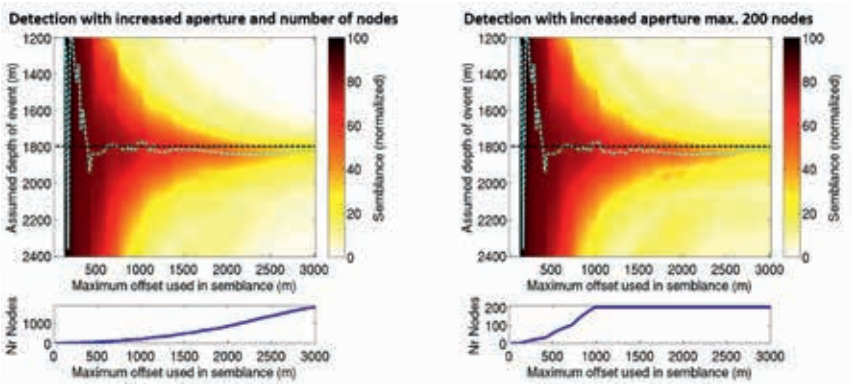

Figure 5 Microseismic detection of the strongest G8 event for different depths at a fixed x-y location. Shown is the semblance at different depths versus an increased array size (maximum offsets used for the semblance detection). The cyan line shows the maximum semblance. On the left, all possible receivers are used, on the right, a maximum of 200 sensors is used. The number of sensors used in the semblance computation is displayed in the lower panels.

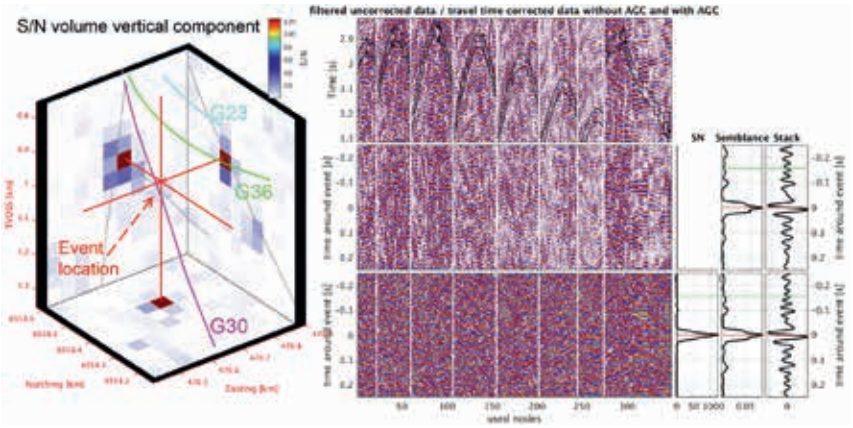

Figure 6 G30 microseismic event with the highest S/N of the semblance weighted stack but with a semblance of only 8.6%. We feel confident in the shown event, because it occurs at the correct location and the right timing. In addition, the event is very focused in the 3D S/N volume (left). Right panel with uncorrected seismic data (top, 5-40 Hz), travel time corrected seismic without (middle) and with applied AGC (bottom). S/N, semblance and stack curves to the right.

events are real events, and not false. Beside events with a high S/N, events with a high semblance value are detected as well, as shown in Figure 7. The high-semblance events are more visible in the seismic data (see Figure 2) and there is less doubt that these events are real. All events have very low amplitudes with a S/N often far below 1 on a single trace. This highlights the power of the applied detection method.

In general, to determine whether weak detected events are real or not, the location of the event and its focusing within the semblance and S/N volumes are considered. In addition, the event time is correlated with injection data. Microseismic events occur often in connection with tiny pressure drops or changes in the injection rate, so the injection data provide an independent evaluation tool to determine whether a detected event is real. In the case of the G30 well, all detected events are visually inspected, and classified as 'real' or 'false', based on their location and focusing of the semblance and S/N volumes. Since G30 is not an injection well, data from the well operation have been correlated with microseismic event times. Parameters like weight on bit (WOB) or rotation per minute (RPM) do not correlate with the occurrence of events. In contrast, the bit depth and the applied torque correlate well as shown in Figure 8. Many events occur when the applied torque is high, whereas no real events are detected at lower torques. The good agreement of event times and high torque values strongly suggest that the detected real events are correlated to the well operation.

The detected events are not located at the toe of the open hole, where the drill bit drills into the cement plug. They occur around 200 m shallower at the depth of the top cut of the inner casing. The inner well diameter is smaller at the top cut location and it is likely that the drill string is 'touching' the top cut which creates noise/microseismic data. So, no fracturing occurs in the formation. Being able to detect such weak drilling noise is a confirmation for the functionality and sensitivity of the real-time microseismic event detection system, and this gives us confidence that the system should be able to detect major caprock failure and injection-related events, if they would occur.

Independently from the origin of the G30 events, they have been used for benchmarking of different detection methods, filtering techniques and processing steps (see Table 1). Taking a semblance-based detection method as a base case, and using only bandpass filtering in the pre-processing, we detected 382 events within seven hours. However, only 131 of them are real events, while 251 are classified as false. The large amount of false detections within that short time period does not provide a practical detection method, as it is impossible to QC all these events. Going over to detection based on the combination of semblance and S/N of the semblance-weighted stack, together with applying the FX filter in the pre-processing flow, reduces the amount of false detection by a third and the number of real events is increased to 178. By adding the subspace filter to the pre-processing flow, a similar large improvement is achieved: Now we are left with only a few false detections and nearly double as many real events compared to the strict semblance-based detection. These remaining false events are all related to the strong seismic interference noise. Figure 8 presents the false/true detections before/after the subspace filter. In general, false events occur only during periods with seismic interference noise

Detection method	Filter and processing			Event detection			
	FX	Subspace	Static	Total	False	Real	Visible in seismic
Semblance				382	251	131	not evaluated
Semblance & S/N of semblance-weighted stack	X			264	86 (- 65%)	178 (+ 36%)	69
Semblance & S/N of semblance-weighted stack	X	X		242	16 (- 94%)	226 (+ 73%)	145
Semblance & S/N of semblance-weighted stack	X	X	X	315	9 (- 96%)	306 (+ 134 %)	237

Table 1 Summary of benchmark results of different detection algorithms, filtering techniques and processing steps. Detected events are manually inspected, and classified as 'real' or 'false' and if visible (subjective evaluation) in the seismic.

as visible in the comparison with the spectrogram in Figure 8 and they are independent from the well operation.

A final improvement can be achieved by applying a static correction to the data which considers small velocity variations. These velocity variations are assumed to be mainly shallow and are not present in the smooth velocity model used for migrating the active seismic data, and used here to compute the travel times. The challenge is to estimate a good static correction. Detected events, not visible at all in the data (Figure 6), cannot be used. Events with higher semblance values as shown in Figure 7, cannot be used either, as their amplitudes are still too small for a static calculation. Therefore, we have chosen to stack events. Under the assumption that the event type is the same for all events related to the G30 P&A operation, all travel time corrected data can be stacked to increase the S/N of the event stack. Figure 9 shows the stack of 90 events, originating from the same voxel before and after applying the static correction. When the static correction is included in the processing flow, the number of detected events is further increased (Table 1).

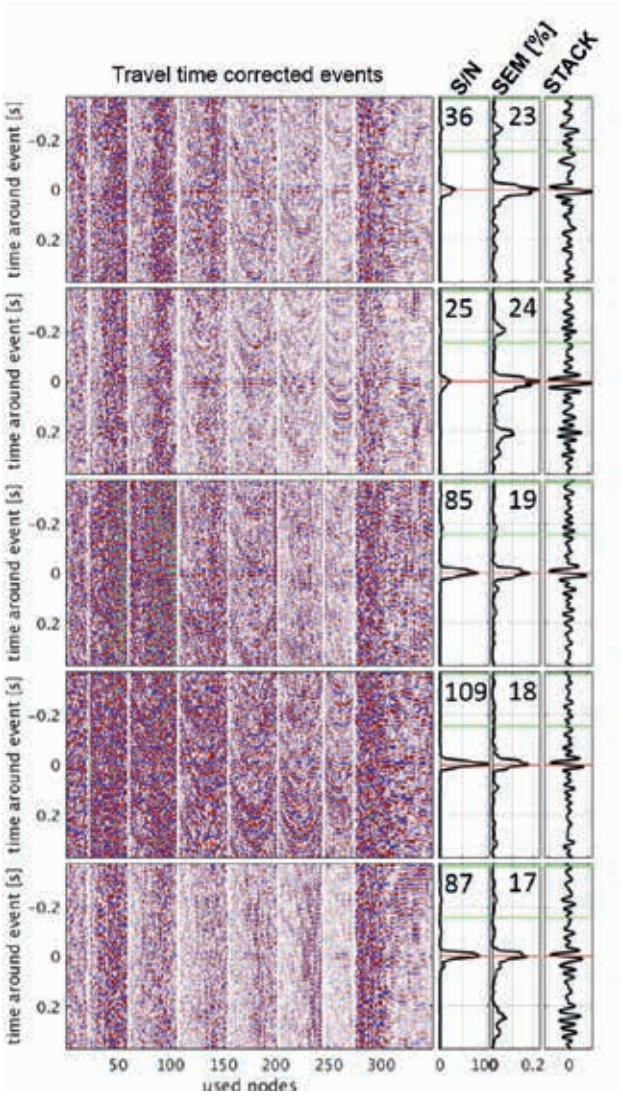

Figure 7 Microseismic events with highest semblance values, but relatively low S/N ratios within various noise situations. Events are clearly visible in the 5-40Hz filtered and travel time corrected seismic data (left) and in the semblance curve (middle panel) whereas the stack (right panel) emphasizes the events only slightly. (Subspace filter and static included; Signal (red line)-to-noise (between green lines) window.)

During the processing of the G30 data, only P-events have been recorded. The event stack can be used to enhance possible S-events, even if they are not detected owing to a possibly incorrect S-wave velocity model. Correcting the data from the horizontal components for the P travel-times, followed by a stack over all events, should enhance possible S-wave energy, even if the S-event is not flat. But not even that trick could reveal some shear energy within the data set.

Table 1 shows the summary of the benchmarking. Every additional improvement has led to a reduction of false events and to an increased number of real events. Around 95% of the false events could be avoided compared to the base case and the number of real events was more than doubled. A large number of events became actually visible in the seismic, after all available pre-processing steps have been applied.

Detection of earthquakes

Norway is the main seismically active zone in northern Europe away from the tectonic plate boundaries. The majority of seismicity in Norway is associated with the Norwegian continental shelf (NCS) (Figure 10). Dense tectonic seismicity close to major oil/gas fields is aligned along the large geological structures and not related to hydrocarbon production. But owing to the proximity of the seismicity to oil/gas fields, Statoil implemented a requirement to study active faulting to ensure safe operation.

Seismicity in Norway is reported by the Norwegian National Seismic Network (NNSN) and Norsar. Their seismic stations are deployed on land and therefore have limited sensitivity to the smaller earthquakes which may occur offshore in the NCS. Therefore, it is essential to use the permanently deployed

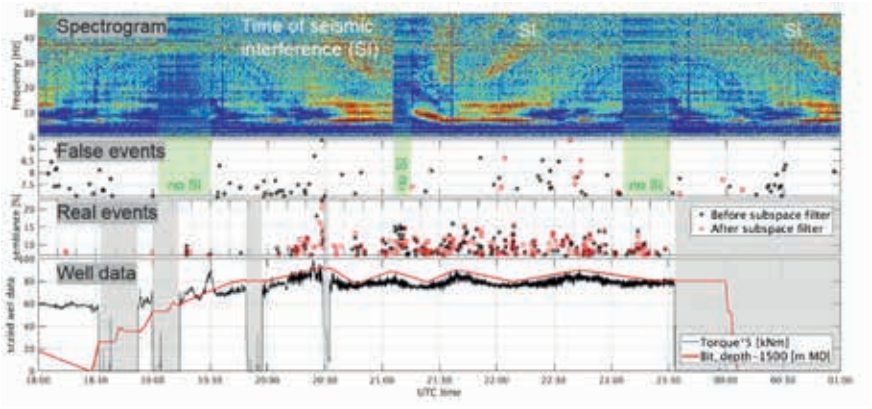

Figure 8 Microseismic events detected during the P&A operation in G30. The spectrogram (top) shows the ambient noise with periods of seismic interference (SI). False and real microseismic events are shown with and without application of the subspace filter (middle panels) and well operation data (bottom).

geophones in the PRM systems to lower the detection threshold of earthquakes near the operational fields. Since summer 2017, several small and moderately sized earthquakes on the NCS have been detected with the Grane PRM system. In addition, large distance events were detected, e.g. the magnitude 8.1 Mexico earthquake (08/09/2017) and the magnitude 6.3 North Korean nuclear test (03/09/2017), which both occurred thousands of kilometres away to the west and the east of the Grane PRM.

For Statoil, earthquake detection on the NCS is most relevant. Ten stations from Grane PRM are selected (Figure 1) in different azimuthal directions to detect earthquakes using the STA/LTA algorithm (Allen, 1978). Although geophones are designed to record active seismic and high-frequency passive events, the response function in lower-frequency signals is good enough to detect earthquakes as well. To avoid false detection in the challenging marine noise environment, we currently use the 'silent' gap in the frequency spectra (2.5-4.5 Hz) between the microseism at low frequencies and the anthropogenic noise at higher frequencies to detect earthquakes in the NCS. An event is flagged as an earthquake, when at least four stations get triggered by the S/N threshold. Since June 2017, seven earthquakes in the vicinity of operational fields in the NCS have been detected, where the magnitude spans between 1.8 and 4.8. Figure 11 shows three earthquakes recorded with Grane PRM sensors, occurring in a major graben structure on 30/06/2017, 14/09/2017, and 30/11/2017 with M4.8, M2.8, and M1.8, respectively. Localization and estimation of the magnitude of these earthquakes is done by NNSN and Norsar. The 30 June 2017 earthquake was located 44 km SW of Grane where the seismic wave propagated towards Grane PRM with the approximate azimuthal direction of 61 degrees. This event was the strongest event in 2017 occurring on the NCS. Detecting the 30 November 2017 earthquake with M1.8, about 78 km SW of Grane PRM shows the sensitivity of PRM geophones to detect even small movements along the fault planes in the NCS. The latter earthquake was as well recorded by NNSN, but not detected owing to low amplitudes on their onshore stations.

Successful detection of earthquakes located in the vicinity of the Grane field encouraged us to run the same system on other PRM systems operated by Statoil (e.g. Oseberg). To promote HSE, safe operation, and improve our understanding of stress

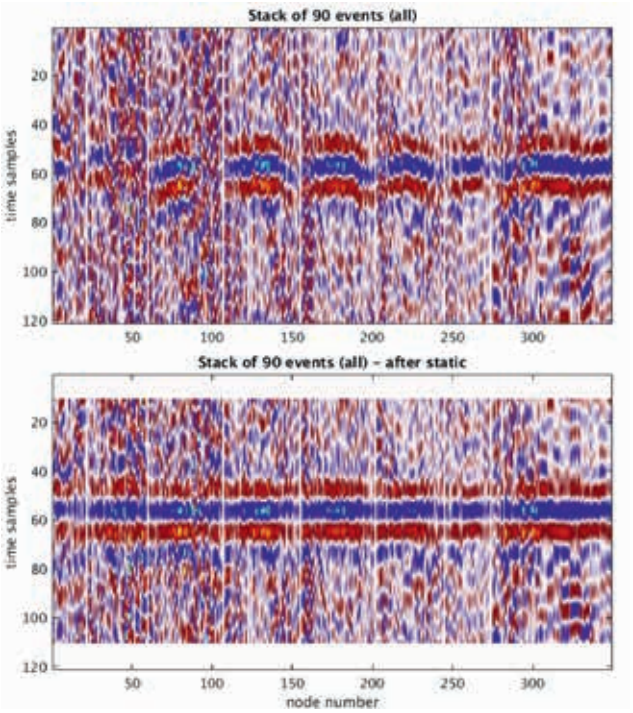

Figure 9 Stack of 90 events, which origin from the same voxel, prior (top) and post (bottom) static correction.

regimes within the NCS, Statoil and its Grane and Oseberg licence partners agreed to start streaming passive seismic data from ten sensors at Grane and ten sensors at Oseberg to the NNSN. Integrating these stations to the onshore seismic network operated by the NNSN has mutual benefits for both Statoil and academia, resulting in a more accurate location and a lower detection threshold for the earthquakes occurring offshore Norway. A close co-operation between Statoil and NNSN is now established.

Conclusion and outlook

In this paper, we have demonstrated the functionality of a real-time injection and overburden surveillance system at the Grane PRM field. In the absence of injection-related events, the functionality of the system was verified with events that were correlated to drilling operations. This has increased the

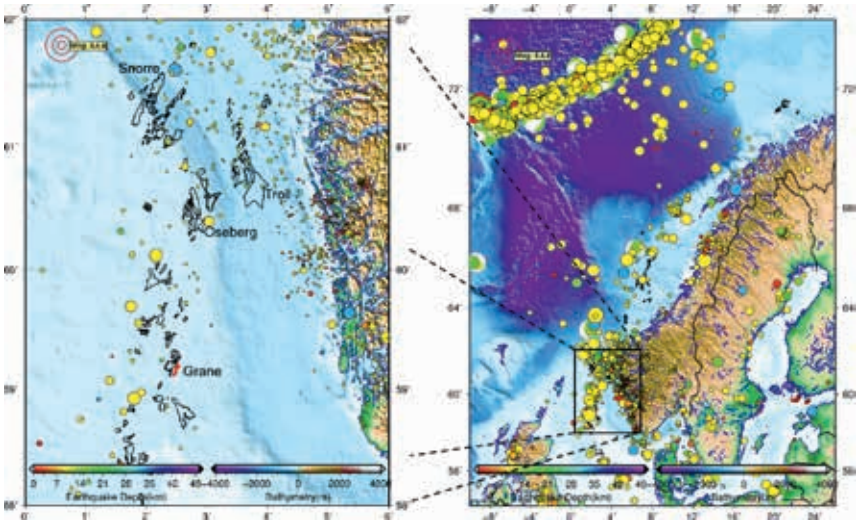

Figure 10 Seismicity in Norway, with the focus in the Norwegian continental shelf since 1986 (USGS). Focal mechanism of large earthquakes collected from Global CMT solution Catalogue, field layouts (black) from NPD.

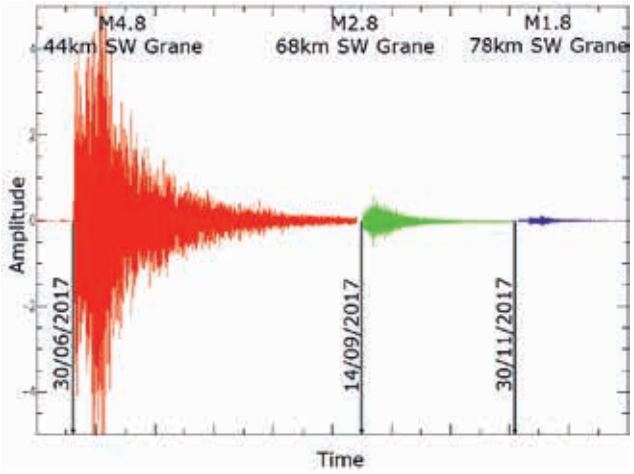

Figure 11 Three earthquakes (vertical component) with different magnitudes located at different distances from Grane.

confidence in the system significantly. Monitoring injectors has clear HSE advantages and might help to extend their lifetime. When cases such as the G8 liner failure happen, a real-time system would be able to save enough costs to pay for the entire monitoring effort.

Based on the G8 microseismic event we have demonstrated that an ideal array size covers a radius of around the depth of the target. Unless no incidents happen, our current experiences show that microseismic events seem to occur mainly during the start-up phase and early life of an injector. It is therefore recommended to start the monitoring process with the first injections. Furthermore, microseismic events can be used to update the velocity model.

The benchmarking test of noise filtering and detection methods highlights that the detection ability has improved significantly and many events with small amplitudes are detected although they are invisible in the seismic data. This raises the question of whether detected events are real. We believe that events are real, even when they are invisible, as long as they are sharply focused in the 4D semblance and the S/N volumes, and when they occur in the vicinity of a well and can be correlated to injection or drilling parameters in that well. When well information is missing, it will be challenging to confirm that weak events are real.

The detection of earthquakes by utilizing only a few nodes will improve our understanding of active faults. It is therefore important to monitor the seismicity around our fields. It is as well an easy way of monitoring the entire field and the surrounding area to detect larger microseismic events than those shown in the examples here.

The microseismic processing flow has demonstrated the reliability regarding detection of even the 'invisible' events. There is potential to improve the localization of events further. Especially precise depth estimates are of high interest. Moment tensor inversions could provide more insight into the event origins. The event stacking might be a good way to allow for these inversions even for the smallest events. A closer follow-up of well operations is desired, and this will hopefully lead to more event detections and increase our experience further. Finally, the achievements can be transferred to other PRM fields.

Microseismic and earthquake detection are motivated by the desire to extract and utilize information contained in passive seismic data, prior to deleting these. However, the passive seismic data contains more than microseismic information, and the potential for using these data for ambient noise analysis, such as interferometry and ambient noise surface wave tomography, will be explored further in the future.

Acknowledgments

We would like to thank Statoil ASA and Grane licence partners: Petoro AS, ExxonMobil E&P Norway AS and ConocoPhillips Skandinavia AS for permission to publish this work. Special thanks also goes to Mats Grønning Andersen, Thomas Johansen, Andreas Amlien Røssland, and Ricardo Jose Martinez Guzman for their valuable contributions to this work. We would also like to thank Rigmor Mette Elde, Richard Tøndel, Grane Petec, and GERI. The views and opinions expressed in this paper are those of the operator and are not necessarily shared by the Grane licence partners.

References

Allen, R.V. [1978]. Automatic earthquake recognition and timing single trace. *Bulletin of Seismological Society of America*, **68**, 1521-1532.

Blunda, Y., and Chambers, K. [2013]. A generic procedure for noise suppression in microseismic data. *CSPG/CSEF/CWLS GeoConvention,* Abstracts.

Bussat, S., Bjerrum, L.W., Dando, B.D.E., Bergfjord, E.V., Iranpour, K., and Oye, V. [2016]. Offshore injection and overburden surveillance using real-time passive seismic. *First Break*, **34**, 51-59.

Caldwell, J., Koudelka, E., Nesteroff, K., Price, R. and Zhang, P. [2015]. Seismic permanent reservoir monitoring (PRM) – A growing market. *First Break*, **33**, 65-73.

Elboth, T., Presterud, I.V. and Hermansen, D. [2010]. Time-frequency seismic data de-noising. *Geophysical Prospecting*, **58**, 441-453, doi: 10.1111/j.1365-2478.2009.00846.x.

Houbiers, M., Bussat, S. and Zarifi, Z. [2018]. Real-time microseismic monitoring at Grane, offshore Norway. *80th EAGE Conference & Exhibition*, Extended Abstracts (submitted).

Jones, I.F. and Levy, S. [1987]. Signal-to-noise ratio enhancement in multichannel seismic data via the Karhunen-Loéve transform. *Geophysical Prospecting*, **35**, 22-32.

Thompson, M., Andersen, M., Elde, R.M., Roy, S.S. and Skogland, S.M. [2015]. The startup of Permanent Reservoir Monitoring for Snorre and Grane. *77th EAGE Conference & Exhibition*, Expanded Abstracts.